Electrochimica Acta 56 (2011) 1123–1129

Contents lists available at ScienceDirect

Electrochimica Acta

journal homepage: www.elsevier.com/locate/electacta

Fabrication of Naphthol green B/layered double hydroxide nanosheets ultrathin film and its application in electrocatalysis

Xianggui Kong, Jingwen Zhao, Jingbin Han, Danyao Zhang, Min Wei*, Xue Duan

State Key Laboratory of Chemical Resource Engineering, Beijing University of Chemical Technology, Beijing 100029, China

ARTICLE INFO

Article history:
Received 10 August 2010
Received in revised form 22 October 2010
Accepted 24 October 2010
Available online 4 November 2010

Keywords:
Layered double hydroxide nanosheets
Naphthol green B
Layer-by-layer self-assembly
Organic–inorganic ultrathin film
Enzyme-free sensor

ABSTRACT

A facile enzyme-free hydrogen peroxide electrochemical sensor was fabricated based on multilayer ultrathin film containing Naphthol green B anions (NGB) and exfoliated nanosheets of Co–Al layered double hydroxide (LDH) *via* layer-by-layer self-assembly technique. The X-ray diffraction pattern indicates the superlattice structure of the film with repeating distance of 4.15 nm; SEM and AFM images show that the film surface is continuous and uniform. The electrochemical behavior of the ultrathin film was studied by cyclic voltammetry and electrochemical impedance spectroscopy. The ultrathin film modified electrode shows a fast direct electron transfer for the Co^{2+}/Co^{3+} redox couple with $\Delta E = 14$ mV in 0.1 M NaOH solution. Furthermore, the modified electrode displays a significant electrocatalytic performance for H_2O_2 with Michaelis–Menten constant $K_M^{app} = 169.3$ μM. The anodic peak current increased linearly with the concentration of H_2O_2 from 8.0×10^{-6} to 1.8×10^{-4} M with a low detection limit of 9.0×10^{-7} M. The NGB/LDH ultrathin film was demonstrated as a feasible electrochemical sensor for detection of H_2O_2 with rapid response, high stability, good reproducibility and excellent selectivity.

1. Introduction

Recently, electrochemical sensors have become one of the most promising analytical tools in medical science, pharmacology research and environmental detection due to their simplicity, high sensitivity and excellent selectivity [1–4]. Significant improvements continue to be made in methodologies and fabrication since the invention of electrochemical sensor. Considerable research interests have been focused on the subject of how to modify the electrodes for the purpose of obtaining electrochemical sensors with high stability, sensitivity and specificity [5–7]. Various methods including electrochemical deposition, screen-printing technique, sol–gel technique and spin-coating approach, have been widely used and made great achievements in modifying electrodes [8–11]. More recently, the electrostatic layer-by-layer (LBL) self-assembly method has attracted much attention owing to the controllability of desirable thickness and architecture at a nanometer level. Some multilayer ultrathin films (UTFs) fabricated by LBL method have been extensively applied in electrochemical sensors [12–15]. Among them, the inorganic–organic UTFs have become the intense research target attributed to their high stability, good biocompatibility and eminent conductivity [16–19].

Layered double hydroxides (LDHs), well-known as an important class of inorganic layered material, can be represented by the general formula $[M^{2+}_{1-x}M^{3+}_x(OH)_2]^{x+}(A^{n-})_{x/n}\cdot mH_2O$, where M^{2+} and M^{3+} are divalent and trivalent metal ions respectively, and A^{n-} is an exchangeable anion compensating for the positive charge of the hydroxide layers [20–23]. In recent years, LDHs, especially containing transition metals, have become the potentially attractive materials for electrode surface modifications due to the charge transport, redox catalysts, anion exchange and biocompatible properties [24–27]. However, further application was largely restricted because many macromolecules (enzymes and other electroactive molecules) cannot be intercalated into the LDH gallery but only absorbed onto the surface of LDH particles, resulting in low loading, serious aggregation as well as desorption. In addition, the generally used drop-casting method for the modification of electrodes leads to poor adhesion of LDH particles to the substrate.

Recently, extensive efforts have been directed toward the delamination of LDH to obtain positively charged single nanosheets with ultimate 2D anisotropy [28–30]. One of the most important and attractive applications of such exfoliated nanosheets is that they serve as 2D building blocks to construct organic–inorganic ultrathin films with superior functionalities to individual component [31,32]. This therefore inspires us to fabricate the electrochemical sensor by alternate LBL assembly of positively charged LDH nanosheets and negatively charged electroactive species. The resulting ultrathin film would exhibit the following advantages: firstly, the molecular level of assembly will result in a

* Corresponding author. Tel.: +86 10 64412131; fax: +86 10 64425385.
E-mail addresses: weimin@mail.buct.edu.cn, weimin-hewei@163.com (M. Wei).

0013-4686/$ – see front matter © 2010 Elsevier Ltd. All rights reserved.
doi:10.1016/j.electacta.2010.10.081

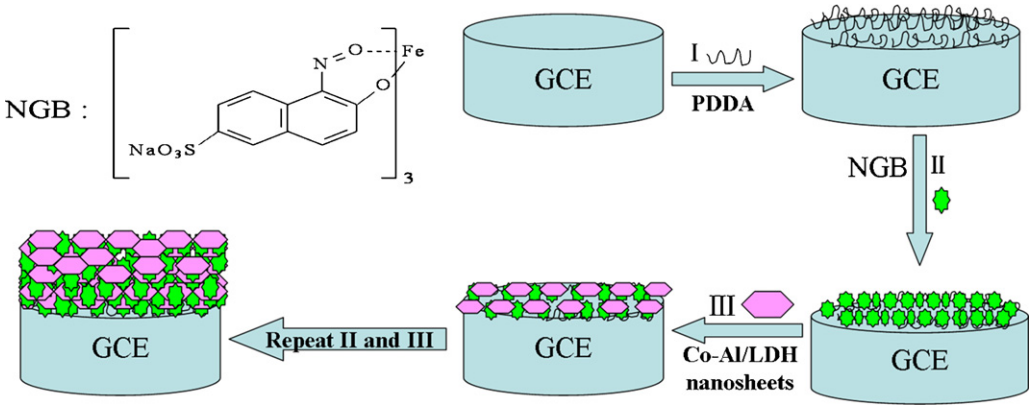

Fig. 1. Schematic representation for the LBL assembly of $(NGB/LDH)_n$ UTFs.

fast electron transfer between redox species and the underlying electrode owing to the high dispersion and uniform orientation of electroactive substance; secondly, the incorporation of LDH nanosheets can improve the adhesion of the ultrathin film to the electrode and thus facilitate the stability over a long period of usage.

In this work, a novel enzyme-free electrochemical sensor was fabricated based on UTFs composed of Co–Al LDH nanosheets and Naphthol green B (NGB, Fig. 1) *via* the electrostatic LBL assembly on the glass carbon electrode (GCE). Herein, Co–Al LDH nanosheets worked as building blocks as well as electroactive substance and NGB, which was often used as a mediator in electrocatalysis [33,34], served as negatively charged counterpart. The NGB/LDH UTF modified electrode was characterized by cyclic voltammetry and its electrocatalytic behavior for the oxidation of H_2O_2 was thoroughly studied. We hope that the novel strategy in this work provides a feasible method for fabricating organic–inorganic UTFs with superior electrochemical properties, for the purpose of potential applications in electroanalysis and electrochemical sensors.

2. Experimental

2.1. Materials and reagents

Poly(styrene sulfonic acid) (PSS, MW = 70,000), Naphthol green B (NGB) and an aqueous solution (20%) of poly(diallydimethylammonium chloride) (PDDA, MW: 100,000–200,000) were purchased from Alfa Aesar Chemical Co. Ltd. All other chemicals were of analytical grade and used without further purification. All the solutions were prepared by using water purified in a Milli-Q Millipore system (>18 MΩ cm).

2.2. Fabrication of the multilayer UTFs

The Co–Al LDH nanosheets were prepared according to the reported method [28]. The detailed synthesis and characterization of Co–Al LDH and Co–Al LDH nanosheets were described in ESI (Figs. S1 and S2). The $(NGB/LDH)_n$ UTFs were fabricated by applying the LBL assembly technique. Prior to assembly, the GCE (3 mm, diameter) was polished successively with 1.0, 0.3, and 0.05 μm alumina powder, and sonicated in 1:1 nitric acid/water, absolute ethanol and Milli-Q water for 1 min respectively. The cleaned GCE was firstly dipped into a PDDA solution (PDDA:H_2O = 1:20, v/v) for 20 min and then washed thoroughly and dried with a N_2 flow. The fabrication of the $(NGB/LDH)_n$ multilayer films was carried out according to the following steps: the pretreated substrates were dipped alternately into the negatively charged NGB solution (1 mg mL^{-1}) and the colloidal suspension of Co–Al LDH nanosheets (1 mg mL^{-1}), for 10 min each time. After each assembly step, the substrates were thoroughly rinsed with deionized water and dried with a N_2 flow. Subsequently, a series of deposition operations for NGB and LDH nanosheets were repeated *n* times to obtain $(NGB/LDH)_n$ UTFs (Fig. 1). The fabrication process of the $(NGB/LDH)_n$ UTFs that deposited on quartz glass is similar to that described above. Quartz glass (3.0 cm × 1.0 cm) substrates were cleaned by immersing in a fresh piranha solution (H_2SO_4:H_2O_2 (30%) = 3:1, v/v) (*warning*: piranha solution is very corrosive and must be treated with extreme care) for 30 min, followed by rinsing in deionized water and drying with a N_2 flow.

2.3. Characterization and amperometric measurements

X-ray diffraction (XRD) patterns were recorded by a Rigaku XRD-6000 diffractometer, using Cu Kα radiation (λ = 0.15418 nm) at 40 kV, 30 mA. The UV–vis spectra were collected in a Shimadzu U-3000 spectrophotometer. The morphology of thin films was investigated using a scanning electron microscope (SEM Hitachi S-4700) with the accelerating voltage of 20 kV. The surface roughness was studied using the atomic force microscopy (AFM) software (Digital Instruments, Version 6.12).

The electrochemical measurements were performed using a CHI 660C electrochemical workstation (Shanghai Chenhua Instrument Co., China). A conventional three-electrode system was used, including a modified GCE as the working electrode, a platinum foil as the auxiliary electrode and a saturated Ag/AgCl electrode as the reference electrode. Electrochemical impedance spectroscopy (EIS) measurements were performed on $(NGB/LDH)_n$ modified electrodes in 0.1 M NaOH with 5 mM $Fe(CN)_6^{3-/4-}$ solution at a potential of +0.22 V *vs.* Ag/AgCl. The EIS dispersions were recorded in the frequency range 0.01–100 kHz. The solutions were purged with highly purified nitrogen for 20 min prior to measurement. All measurements were performed at room temperature.

3. Results and discussion

3.1. Structural and morphological characterization of the $(NGB/LDH)_n$ UTFs

The multilayer film buildup process was monitored with a UV–vis spectrometer after each deposition of NGB as depicted in Fig. 2A. The strong absorption bands at 239 and 292 nm are due to the π–π* transition in the naphthoquinone structure of NGB. Compared with the pristine NGB in aqueous solution (Fig. 2A inset a, 235 and 283 nm), a little red-shift for the multilayer film can be attributed to interactions between individual molecules in the densely packed films. The intensities of the absorption bands at 239 and 292 nm correlate linearly with the bilayers number

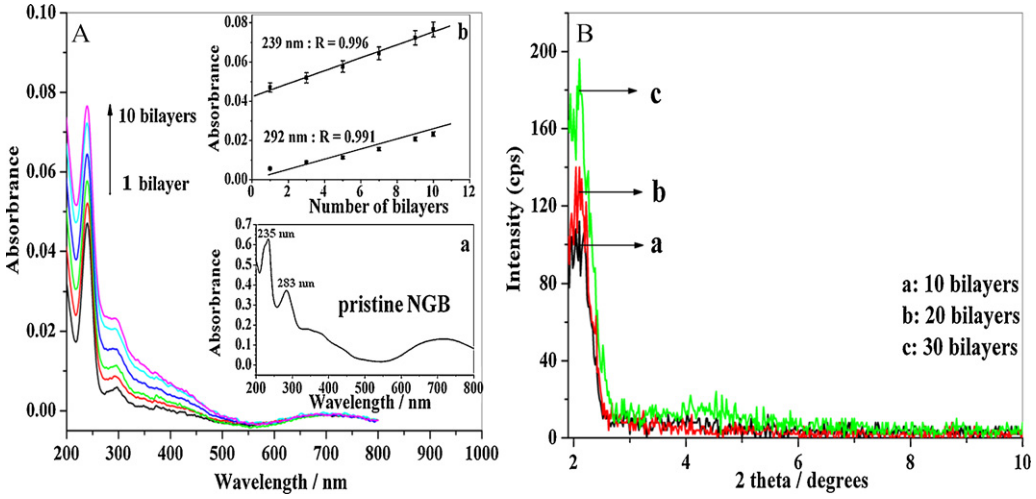

Fig. 2. (A) UV–vis absorption spectra of the $(NGB/LDH)_n$ UTFs along with different bilayer number (n: 1, 3, 5, 7, 9, 10) on quartz glass substrates. The inset a shows the absorption spectrum of pristine NGB (10^{-5} mg mL^{-1}) and the inset b displays plots of the absorbance at 239 and 292 nm *vs.* n respectively; (B) XRD patterns for the $(NGB/LDH)_n$ UTFs deposited on quartz glass substrates.

(Fig. 2A inset b), indicating a stepwise and uniform film growth procedure. XRD patterns (Fig. 2B) of the multilayer films illustrate the evolution of a Bragg peak at $2\theta = 2.1^\circ$ ($d_{001} = 4.1$ nm), which can be attributed to a so-called superlattice reflection of the organic–inorganic periodic nanostructure [30]. Furthermore, the reflection intensity increased progressively with the increase of bilayers number, further confirming the successful fabrication of the $(NGB/LDH)_n$ UTFs.

Further surface morphology and architecture of the $(NGB/LDH)_n$ UTFs were investigated by SEM and AFM. The top view of SEM images for the $(NGB/LDH)_n$ UTFs showed that both the homogeneity and surface coverage of the UTFs increased with the increase of bilayer number (Fig. 3A). AFM topographical images (3 μm × 3 μm) of the $(NGB/LDH)_n$ UTFs are shown in Fig. 3B. The value of root-mean-square (rms) roughness for the UTFs increased slowly from 2.87 nm (5 bilayers) to 6.98 nm (20 bilayers), indicating relatively smooth surface of the UTFs. Moreover, a linear correlation between the film thickness and bilayer number was observed from their side view SEM images (Fig. S3), confirming that the UTFs possess a uniform and periodic layered structure. The thickness of one bilayer was calculated to be ~3.9 nm from the linear slope, in approximate agreement with the periodicity result obtained from XRD measurement (4.1 nm).

3.2. Direct electrochemistry of the UTFs modified electrode

Cyclic voltammograms (CVs) in 0.1 M NaOH solution of the bare electrode, the $(NGB/PDDA)_6$ UTF modified and the $(NGB/LDH)_6$ UTF modified electrode are displayed in Fig. 4A. No redox peaks were observed both for the bare electrode and the $(NGB/PDDA)_6$ UTF modified electrode (curve a and b respectively). However, the $(NGB/LDH)_6$ UTF modified electrode gives a couple of well-defined reversible redox peaks at 0.496 and 0.482 V respectively (curve c). These observations clearly demonstrate that this pair of peaks

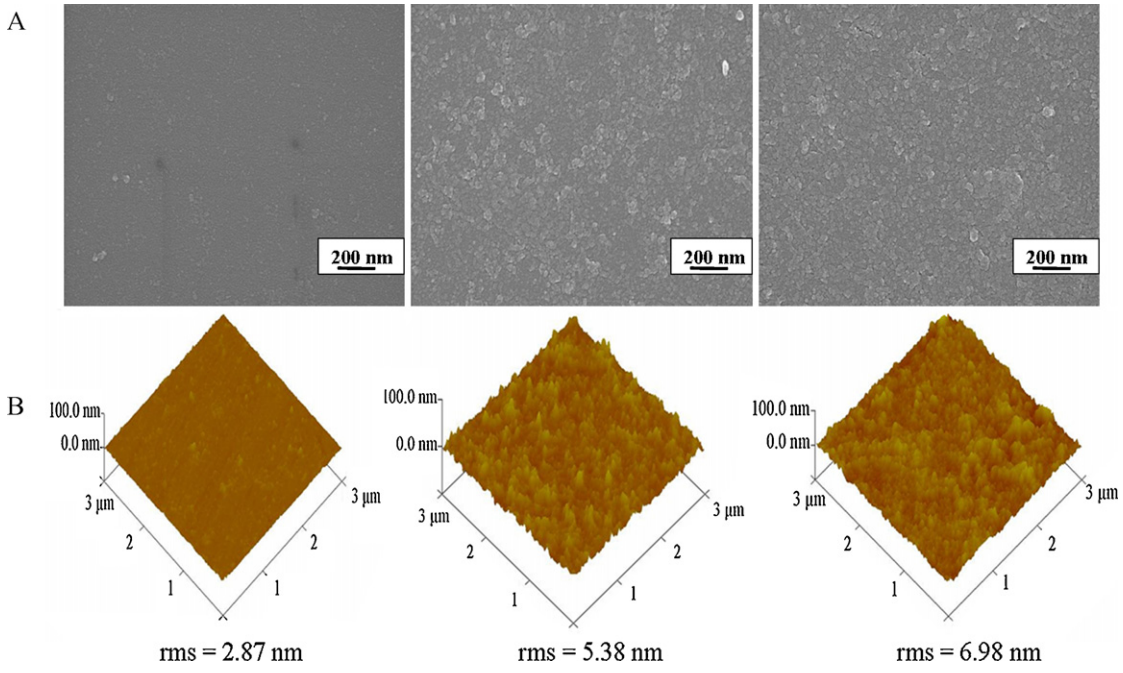

Fig. 3. (A) Top view of SEM images for the $(NGB/LDH)_n$ UTFs (n = 5, 10, 20); (B) AFM images of the $(NGB/LDH)_n$ UTFs (n = 5, 10, 20).

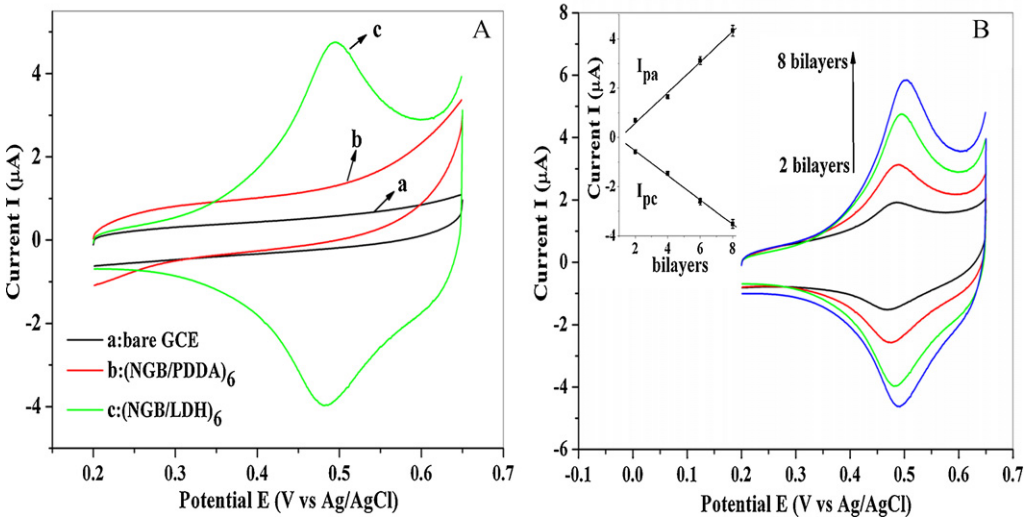

Fig. 4. (A) CVs of bare GCE, the $(NGB/PDDA)_6$ modified electrode and $(NGB/LDH)_6$ modified electrode in 0.1 M NaOH at a scan rate of 0.1 V s^{-1}; (B) CVs of the $(NGB/LDH)_n$ modified electrode with different bilayer number (n): 2, 4, 6 and 8 in 0.1 M NaOH at a scan rate of 0.1 V s^{-1}. The inset shows the plots of I_{pa} and I_{pc} *vs.* n respectively.

belongs to the redox reaction of Co–Al LDH nanosheets. Moreover, a rather low ΔE_p (14 mV) was obtained for the $(NGB/LDH)_6$ modified electrode, and the ratio between the anodic and cathodic peak current was ~1.2. Compared with the $(NGB/LDH)_6$ modified electrode, the $(PSS/LDH)_6$ modified electrode gave a couple of not well-resolved redox peaks at 0.536 and 0.434 V under the same conditions with ΔE_p = 92 mV (Fig. S4), indicating that NGB serves as a kind of conductive substance facilitating charge transfer. Furthermore, the CVs of $(NGB/LDH)_n$ modified electrodes with different bilayer numbers are shown in Fig. 4B, from which the peak current (both anodic and cathodic) exhibits linear augment along with the bilayer number (n), suggesting the uniform growth of the $(NGB/LDH)_n$ UTFs. In addition, Fig. S5 shows CVs of the $(NGB/LDH)_6$ modified electrode performed at different pH values. As the pH value increases, the peak potential shifts to negative direction with a slope of −70.2 mV pH^{-1}, indicating a transfer of two-proton (OH^-) process in the pH range 12–13. Similar result has also been reported by Tian et al. [35] and the peak current increases simultaneously, suggesting that OH^- plays a key role in the redox process of cobalt. According to the previous reports on the redox reaction of Co^{2+}/Co^{3+} in Co–Al LDH in 0.1 M NaOH solution [25,36], the redox reaction in this system can be described as Eq. (1):

$$Co(OH)_2\text{–LDH} + OH^- \leftrightarrow CoOOH\text{–LDH} + H_2O + e^- \quad (1)$$

Electrochemical impedance spectroscopy (EIS) is an effective method for probing the features of surface-modified electrodes and has been successfully used to characterize the formation of multilayer films on different substrates [37,38]. The EIS consists of two sections: one is the linear part at lower frequencies representing the diffusion-limited process; the other one is a semicircle portion observed at higher frequencies corresponding to the electron-transfer-limited process. The Nyquist plots of the bare electrode and the $(NGB/LDH)_n$ UTF modified electrodes with different bilayers are shown in Fig. 5. The bare electrode exhibits a straight line, which is a characteristic of diffusion limited electrochemical process. In contrast, a semicircle part of the impedance spectrum can be observed for the $(NGB/LDH)_n$ UTF modified electrode and the diameters of the semicircle increased with the increase of bilayer number, indicating the augment of electron-transfer resistance along with the deposition procedure. The results above confirm a successful LBL growth of the $(NGB/LDH)_n$ UTF on the surface of GCE.

The effect of scan rate on the electrochemical response of the modified electrode is displayed in Fig. 6A. The redox peak current increased linearly with the increase of the scan rate from 0.02 to 0.14 V s^{-1}, indicating that the redox reaction is a surface-controlled electrochemical process. Furthermore, according to the Laviron theory [39,40], the electron transfer coefficient (α) and the electron transfer rate constant (k_s) for the $(NGB/LDH)_n$ modified electrode and $(PSS/LDH)_n$ modified electrode were calculated by the following equations:

$$E_{pa} = E^{\theta'} + 2.303\left[\frac{RT}{(1-\alpha)nF}\right]\log \nu \quad (2)$$

$$E_{pc} = E^{\theta'} - 2.303\left(\frac{RT}{\alpha nF}\right)\log \nu \quad (3)$$

$$\log k_s = \alpha \log(1-\alpha) + (1-\alpha)\log \alpha - \log\left(\frac{RT}{nF\nu}\right) - \frac{nF\Delta E_p \alpha(1-\alpha)}{2.303RT} \quad (4)$$

where α is the charge transfer coefficient; k_s is the electron transfer rate constant; ν is the scan rate; n is number of transferred electron; R is the gas constant; F is the Faraday constant; T is the absolute temperature; $E^{\theta'}$ is the apparent formal potential. Based

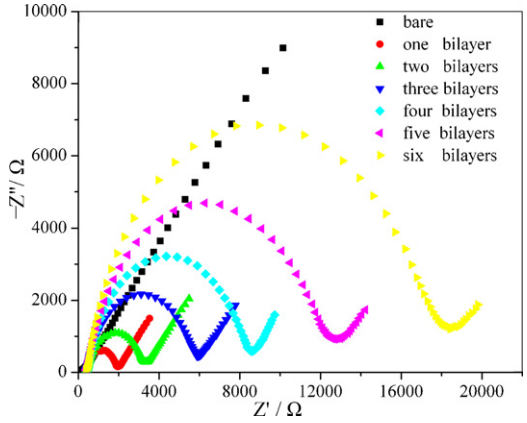

Fig. 5. Nyquist plots of electrochemical impedance spectroscopy for bare GCE and the $(NGB/LDH)_n$ UTF modified GCE with different bilayer number (n): 1, 2, 3, 4, 5 and 6 in 5 mM $Fe(CN)_6^{3-/4-}$ solution.

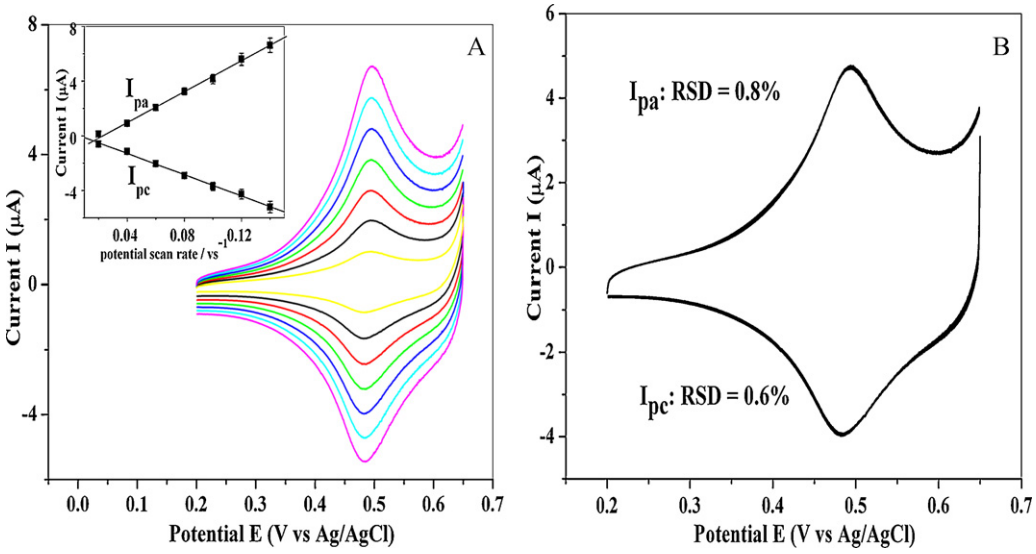

Fig. 6. (A) CVs of the $(NGB/LDH)_6$ modified electrode with scan rate ranging from 0.02 to 0.14 V s^{-1}; inset: plots of peak current *vs.* scan rate in 0.1 M NaOH. (B) The stability of the $(NGB/LDH)_6$ modified electrode in 0.1 M NaOH at a scan rate of 0.1 V s^{-1} for 40 consecutive cycles.

on the linear relationship between E_p and log v (Fig. S6) and Eq. (4), it was calculated that $\alpha = 0.48$ and $k_s = 1.4\ s^{-1}$ for the $(NGB/LDH)_n$ UTF modified electrode; $\alpha = 0.59$ and $k_s = 0.9\ s^{-1}$ for the $(PSS/LDH)_n$ UTF modified electrode. The results demonstrate that NGB accelerates the direct electron transfer between LDH nanosheets and the GCE than PSS. Moreover, the peak potentials of the $(NGB/LDH)_n$ UTF modified electrode were nearly independent on the scan rate in the range 0.02–0.14 V s^{-1}, also demonstrating the NGB accelerated the electron transfer between Co–Al LDH nanosheets and the GCE. Furthermore, the stability of the UTFs was evaluated by consecutive voltammetric sweep method. After 40 consecutive cycles scanning, the relative standard deviation (RSD) was 0.8% for the anodic current and 0.6% for the cathodic current (Fig. 6B), indicating excellent stability of the $(NGB/LDH)_6$ UTF modified electrode.

3.3. Electrocatalytic behavior of the $(NGB/LDH)_6$ UTF modified electrode for H_2O_2

The electrocatalytic behavior of the $(NGB/LDH)_n$ modified electrode towards the electrochemical oxidation of H_2O_2 was investigated by CVs. Fig. S7 shows the response current of different bilayers in the same concentration of H_2O_2, from which the maximum current response for H_2O_2 was obtained at the $(NGB/LDH)_6$ modified electrode. Therefore, the $(NGB/LDH)_6$ UTF modified electrode was chosen as the working electrode in this work.

Fig. 7A shows the CVs of the $(NGB/LDH)_6$ modified electrode in the absence and presence of H_2O_2. A remarkable increase in anodic peak current was observed after the addition of 0.1 mM H_2O_2, with a negative shift for the anodic peak from 0.496 V to 0.394 V. In contrast, no obvious current response was obtained for the bare electrode and the $(NGB/PDDA)_6$ modified electrode under the same conditions (Fig. 7B). The results elucidate that the $(NGB/LDH)_6$ UTF modified electrode exhibits excellent electrocatalytic activity to H_2O_2 and H_2O_2 participates and accelerates the redox reaction of Co–Al LDH on the surface of GCE. Based on the previous reports [25,27] and the results above, it is proposed that the electrochemical reaction process can be described as the following equations:

$$Co(OH)_2\text{–LDH} + OH^- \leftrightarrow CoOOH\text{–LDH} + H_2O + e^- \quad (1)$$

$$CoOOH\text{–LDH} + H_2O_2 + OH^- \rightarrow CoO_2 + 2H_2O + 1/2O_2 + e^- \quad (5)$$

$$CoO_2 + H_2O + e^- \rightarrow CoOOH\text{–LDH} + OH^- \quad (6)$$

The amperometric response of the $(NGB/LDH)_6$ modified electrode to H_2O_2 was examined by successively increasing the

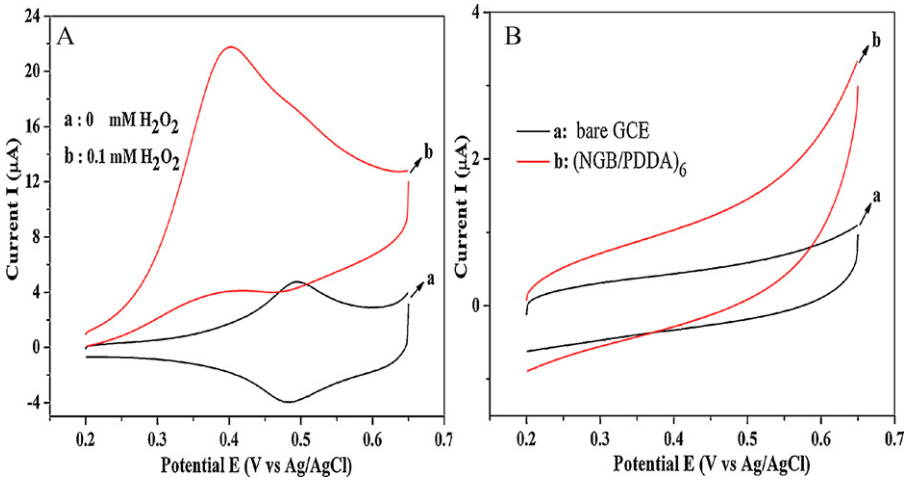

Fig. 7. (A) CVs for the $(NGB/LDH)_6$ modified electrode in the absence and presence of 0.1 mM H_2O_2 at scan rate of 0.1 V s^{-1}; (B) CVs for bare GCE and the $(NGB/PDDA)_6$ modified electrode in the presence of 0.1 mM H_2O_2 at scan rate of 0.1 V s^{-1}.

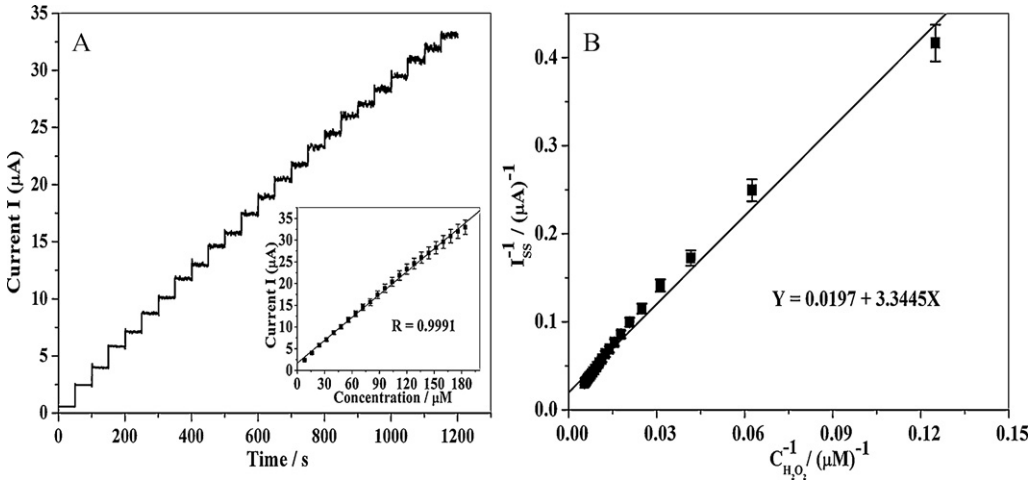

Fig. 8. (A) Typical amperometric response of the $(NGB/LDH)_6$ modified electrode to successive addition of 8 μM H_2O_2 into 0.1 M NaOH solution. Applied potential was 0.38 V. Inset: the calibration curve of *I*–*C* obtained by chronoamperometry; (B) the linear calibration curve of $1/I_{ss}$ *vs.* $C_{H_2O_2}^{-1}$.

concentration of H_2O_2 at the constant potential of 0.38 V (Fig. 8A). A linear relationship between anodic current and the concentration of H_2O_2 was observed with the coefficient of 0.9991 when the concentration of H_2O_2 ranges from 8×10^{-6} to 1.8×10^{-4} M (Fig. 8A inset). The detection limit is estimated to be as low as 0.9 μM (signal over noise $S/N = 3$). The required time to reach 95% steady-state response was 2.7 s, indicating a fast diffusion of H_2O_2 through the UTFs. In addition, the electrocatalytic activity of the $(PSS/LDH)_6$ modified electrode was also investigated (Fig. S8A), and the result shows that the response current is much weaker than that of the $(NGB/LDH)_6$ modified electrode with the same H_2O_2 concentration. This indicates that the electrocatalytic activity of the $(NGB/LDH)_6$ electrode is much higher than that of the $(PSS/LDH)_6$ electrode. Moreover, the response time for the $(NGB/LDH)_6$ electrode (2.7 s) is shorter than that of the $(PSS/LDH)_6$ electrode (5.8 s). Furthermore, it is well known that a smaller Michaelis–Menten constant (K_M^{app}) implies a higher catalytic activity of the immobilized electrocatalyst [41,42]. Herein, a stimulant constant was used to evaluate the electrocatalytic activity of the UTF for H_2O_2. The apparent K_M^{app} can be calculated from the electrochemical version of Lineweaver–Burk equation:

$$\frac{1}{I_{ss}} = \frac{1}{I_{max}} + \frac{K_M^{app}}{I_{max}C} \quad (7)$$

I_{ss} is the steady-state current after the addition of substrate; I_{max} is the maximum current measured under saturated substrate condition; *C* is the bulk concentration of the substrate. Based on the slope and intercept of the linear correlation between the reciprocals of I_{ss} and *C* (Fig. 8B, Fig. S8B), the apparent K_M^{app} was calculated to be 169.3 and 202.6 μM for the $(NGB/LDH)_6$ electrode and $(PSS/LDH)_6$ electrode respectively, indicating that the former electrode exhibits a higher electrocatalytic activity for H_2O_2 than the latter electrode.

Selectivity plays a vital role in practical use for sensors due to the objective always mixed with various interfering substrates. In order to study the selectivity of the $(NGB/LDH)_6$ modified electrode, the interference effect of uric acid, ascorbic acid, glucose and dopamine was examined respectively during amperometric response for H_2O_2 (shown in Fig. 9). A sharp increase in current was obtained with the addition of 0.04 mM H_2O_2; on the contrary, no obvious current response was observed with the addition of either of the interference compounds mentioned above, although the concentration is 10 times higher than that of H_2O_2. In addition, the stability and reproducibility of the sensor were also evaluated. Eight replicate measurements of one electrode over 0.04 mM H_2O_2 show a RSD of 0.9%. The long-term stability was investigated by

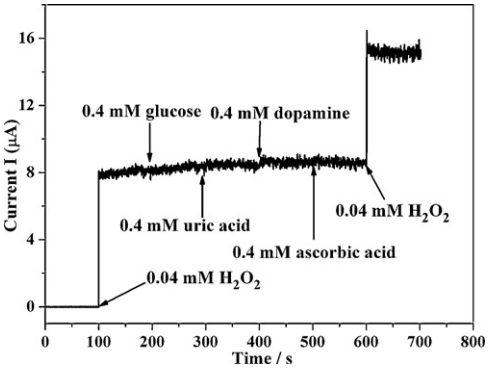

Fig. 9. Current response obtained at the $(NGB/LDH)_6$ modified electrode for the additions of 0.04 mM H_2O_2 and respective 0.4 mM interference compounds into 0.1 M NaOH solution. Applied potential was 0.38 V.

measuring the current response of 0.04 mM H_2O_2 every day over 14 days. After two weeks, the current maintained 92% of its initial response. Furthermore, the reproducibility was evaluated by using five sensors fabricated independently, indicating an acceptable reproducibility with RSD of 1.9% for determining the same concentration of H_2O_2. The results above demonstrate that the $(NGB/LDH)_6$ UTF modified electrode has potential application in the determination of H_2O_2.

4. Conclusions

In summary, organic–inorganic UTFs involving two different electroactive species, NGB and Co–Al LDH nanosheets, were successfully fabricated by LBL technique. The structural and surface morphology studies show that the ultrathin film is continuous and uniform, with long range stacking order resulted from a superlattice nanostructure. The $(NGB/LDH)_6$ UTF modified electrode demonstrates a couple of well-defined reversible redox peaks attributed to the electron transfer between Co–Al LDH nanosheets and GCE. Furthermore, the UTF modified electrode exhibits excellent electrocatalytic activity toward H_2O_2 with a linear response as the concentration of H_2O_2 ranges from 8×10^{-6} to 1.8×10^{-4} M. Furthermore, the long-term stability and the excellent anti-interference performance of the sensor indicate that the $(NGB/LDH)_n$ UTFs will be a promising material for electrochemical sensor application. Therefore, this work provides a facile strategy to fabricate enzyme-free H_2O_2 sensor based on organic–inorganic LBL

self-assembly film. It is anticipated that the method in this work can be used for the design and fabrication of various nano-scale electronic devices or sensors.

Acknowledgments

This project was supported by the National Natural Science Foundation of China, the 111 Project (Grant No. B07004), the 973 Program (Grant No. 2009CB939802) and the Fundamental Research Funds for the Central Universities (Grant No. ZZ0908).

Appendix A. Supplementary data

Supplementary data associated with this article can be found, in the online version, at doi:10.1016/j.electacta.2010.10.081.

References

[1] M.S. Alaejos, F.J.G. Montelongo, Chem. Rev. 104 (2004) 3239.
[2] E. Bakkker, Q. Yu, Anal. Chem. 78 (2006) 3965.
[3] O.A. Sadik, S.K. Mwilu, A.O. Aluoch, Electrochim. Acta 55 (2010) 4287.
[4] X.D. Zeng, X.F. Li, X.Y. Liu, Y. Liu, S.L. Luo, B. Kong, S.L. Yang, W.Z. Wei, Biosens. Bioelectron. 25 (2009) 896.
[5] S. Lupu, C. Lete, M. Marin, N. Totir, P.C. Balaure, Electrochim. Acta 54 (2009) 1932.
[6] O.A. Sadik, A.O. Aluoch, A. Zhou, Biosens. Bioelectron. 24 (2009) 2749.
[7] S. Varma, C.K. Mitra, Electrochem. Commun. 4 (2002) 151.
[8] W. Glatz, L. Durrer, E. Schwyter, C. Hierold, Electrochim. Acta 54 (2008) 755.
[9] W. Yantasee, L.A. Deibler, G.E. Fryxell, C. Timchalk, Y. Lin, Electrochem. Commun. 7 (2005) 1170.
[10] R. Pauliukaite, A.M.C. Paquim, A.M.O. Brett, C.M.A. Brett, Electrochim. Acta 52 (2006) 1.
[11] W. Guo, H.Y. Lu, N.F. Hu, Electrochim. Acta 52 (2006) 123.
[12] Z.Y. Tang, Y. Wang, P. Podsiadlo, N.A. Kotov, Adv. Mater. 18 (2006) 3203.
[13] Z.C. Wang, Z.Y. Li, C.J. Medforth, J.A. Shelnutt, J. Am. Chem. Soc. 129 (2007) 2440.
[14] K. Qiao, H.Y. Liu, N.F. Hu, Electrochim. Acta 53 (2008) 4654.
[15] D. Ragupathy, A.I. Gopalan, K.P. Lee, Microchim. Acta 166 (2009) 303.
[16] M. Du, T. Yang, Y.C. Zhang, K. Jiao, Electroanalysis 21 (2009) 2512.
[17] B.X. Gu, C.X. Xu, G.P. Zhu, S.Q. Liu, L.Y. Chen, M.L. Wang, J.J. Zhu, J. Phys. Chem. B 113 (2009) 6553.
[18] Y.J. Zou, C.L. Xiang, L.X. Sun, F. Xu, Electrochim. Acta 53 (2008) 4089.
[19] P. Wang, Y.X. Li, X. Huang, L. Wang, Talanta 73 (2007) 431.
[20] G.R. Williams, D. O'Hare, J. Mater. Chem. 16 (2006) 3065.
[21] A.M. Fogg, V.M. Green, H.G. Harvey, D. O'are, Adv. Mater. 11 (1999) 1466.
[22] U. Costantino, V. Ambrogi, M. Nocchetti, L. Perioli, Microporous Mesoporous Mater. 107 (2008) 149.
[23] A.M. Fogg, A.J. Freij, G.M. Parkinson, Chem. Mater. 14 (2002) 232.
[24] S. Therias, C. Mousty, Appl. Clay Sci. 10 (1995) 147.
[25] E. Scavetta, M. Berrettoni, F. Nobili, D. Tonelli, Electrochim. Acta 50 (2005) 3305.
[26] S.R. Lee, Y.T. Lee, K. Sawada, H. Takao, M. Ishida, Biosens. Bioelectron. 24 (2008) 410.
[27] E. Scavetta, L. Guadagnini, A. Mignani, D. Tonelli, Electroanalysis 20 (2008) 2199.
[28] L. Li, R.Z. Ma, Y. Ebina, N. Iyi, T. Sasaki, Chem. Mater. 17 (2005) 4386.
[29] Z.P. Liu, R.Z. Ma, M. Osada, N. Iyi, Y. Ebina, K. Takada, T. Sasaki, J. Am. Chem. Soc. 128 (2006) 4872.
[30] R.Z. Ma, K. Takada, K. Fukuda, N. Iyi, Y.S. Bando, T. Sasaki, Angew. Chem. Int. Ed. 120 (2007) 92.
[31] L. Li, R.Z. Ma, Y. Ebina, K. Fukuda, K. Takada, T. Sasaki, J. Am. Chem. Soc. 129 (2007) 8000.
[32] D.P. Yan, J. Lu, M. Wei, J.B. Han, J. Ma, F. Li, D.G. Evans, X. Duan, Angew. Chem. Int. Ed. 121 (2009) 3119.
[33] A.V. Maffei, P.M. Budd, N.B. Mckeown, Langmuir 22 (2006) 4255.
[34] A. Mohadesi, M.A. Taher, Sens. Actuators B 123 (2007) 733.
[35] L. Tian, J.Y. Bian, B.B. Wang, Y.J. Qi, Electrochim. Acta 55 (2010) 3083.
[36] E. Scavetta, A. Mignani, D. Prandstraller, D. Tonelli, Chem. Mater. 19 (2007) 4523.
[37] D.H. Wu, Q. Zhang, X. Chu, H.B. Wang, G.L. Shen, R.Q. Yu, Biosens. Bioelectron. 25 (2010) 1025.
[38] Y.Z. Zhang, H.Y. Ma, K.Y. Zhang, S.J. Zhang, J. Zhang, Electrochim. Acta 54 (2009) 2385.
[39] A. Salimi, H. Mamkhezri, R. Hallaj, S. Zandi, Electrochim. Acta 52 (2007) 6097.
[40] E. Laviron, J. Electroanal. Chem. 52 (1974) 355.
[41] R.A. Kamin, G.S. Wilson, Anal. Chem. 52 (1980) 1198.
[42] M.G. Li, S.H. Chen, F. Ni, Y.L. Wang, L. Wang, Electrochim. Acta 53 (2008) 7255.